UNIVERSITY
OF WOLLONGONG
AUSTRALIA

University of Wollongong
Research Online

Faculty of Informatics - Papers (Archive) Faculty of Engineering and Information Sciences

2011

Automatic Classification of Ground-Penetrating-Radar Signals for Railway-Ballast Assessment

Wenbin Shao
University of Wollongong, wenbin@uow.edu.au

Abdesselam Bouzerdoum
University of Wollongong, bouzer@uow.edu.au

Son Lam Phung
University of Wollongong, phung@uow.edu.au

Lijun Su
University of Wollongong - Dubai Campus, lijun@uow.edu.au

Buddhima Indraratna
University of Wollongong, indra@uow.edu.au

See next page for additional authors

Publication Details

W. Shao, A. Bouzerdoum, S. L. Phung et al., "Automatic Classification of Ground-Penetrating-Radar Signals for Railway-Ballast Assessment," IEEE Transactions on Geoscience and Remote Sensing, vol. 49, no. 10, 2011, pp. 3961-3972. Copyright IEEE 2011. Original item available here

Research Online is the open access institutional repository for the University of Wollongong. For further information contact the UOW Library: research-pubs@uow.edu.au

Automatic Classification of Ground-Penetrating-Radar Signals for Railway-Ballast Assessment

Abstract
The ground-penetrating radar (GPR) has been widely used in many applications. However, the processing and interpretation of the acquired signals remain challenging tasks since an experienced user is required to manage the entire operation. In this paper, we present an automatic classification system to assess railway-ballast conditions. It is based on the extraction of magnitude spectra at salient frequencies and their classification using support vector machines. The system is evaluated on real-world railway GPR data. The experimental results show that the proposed method efficiently represents the GPR signal using a small number of coefficients and achieves a high classification rate when distinguishing GPR signals reflected by ballasts of different conditions.

Keywords
Ground-penetrating radar (GPR) processing, railway-ballast assessment, support vector machine (SVM)

Disciplines
Physical Sciences and Mathematics

Publication Details
W. Shao, A. Bouzerdoum, S. L. Phung et al., "Automatic Classification of Ground-Penetrating-Radar Signals for Railway-Ballast Assessment," IEEE Transactions on Geoscience and Remote Sensing, vol. 49, no. 10, 2011, pp. 3961-3972. Copyright IEEE 2011. Original item available here

Authors
Wenbin Shao, Abdesselam Bouzerdoum, Son Lam Phung, Lijun Su, Buddhima Indraratna, and Cholachat Rujikiatkamjorn

This journal article is available at Research Online: http://ro.uow.edu.au/infopapers/1247

Automatic classification of ground penetrating radar signals for railway ballast assessment

Wenbin Shao, Abdesselam Bouzerdoum, *Senior Member, IEEE,* Son Lam Phung, *Member, IEEE,* Lijun Su, Buddhima Indraratna, and Cholachat Rujikiatkamjorn

***Abstract*—Ground penetrating radar has been widely used in many applications. However, the processing and interpretation of the acquired signals remain challenging tasks since an experienced user is required to manage the entire operation. In this paper, we present an automatic classification system to assess railway ballast conditions. It is based on the extraction of magnitude spectra at salient frequencies and their classification using support vector machines. The system is evaluated on real-world railway GPR data. The experimental results show that the proposed method efficiently represents the GPR signal using a small number of coefficients, and achieves a high classification rate when distinguishing ground penetrating radar signals reflected by ballast of different conditions.**

***Index Terms*—Railway ballast assessment, ground penetrating radar processing, support vector machine.**

I. Introduction

GROUND penetrating radar (GPR), sometimes called subsurface radar, ground probing radar, georadar or earth sounding radar, exploits electromagnetic fields to probe lossy dielectric materials [1, 2, 3, 4]. It can non-destructively detect buried objects beneath the shallow earth surface (less than 50 m) or in a visually impenetrable structure, such as walls and concrete floors. GPR has attracted considerable interest in many areas, such as archaeology [5], road construction [6], glacier and ice sheet investigation [7], and mineral exploration and resource evaluation [8].

As a cost-effective and environment-friendly means of transportation, railway plays an important role in daily life. A railway structure typically consists of steel rails, fastening system, sleepers, ballast, subballast and subgrade [9]. The transverse section of a railway is given in Fig. 1. The ballast is an essential component for proper railway functioning. To ensure safety, regular inspection of rail tracks must be conducted. Traditionally, track investigation involves drilling to collect ballast samples from the railway sites. The ballast samples are then sent to a laboratory for assessment, which involves fouling index measurement. Finally, maintenance actions are determined based on the evaluation results. The entire procedure is labor-intensive and time-consuming. Thus, the rail industry is searching for new and more cost-effective approaches. As a non-destructive detection tool, ground penetrating radar has attracted great interest in railway ballast evaluation in recent years [10].

Despite its commercial success, GPR still faces various fundamental problems. Specifically, processing and interpreting radar profiles are still challenging tasks [12, 13]. In addition to traditional GPR processing techniques, such as dewow and filtering, researchers have employed various signal processing techniques to aid the GPR signal analysis and interpretation [2, 13, 14]. For example, Al-Qadi *et al*. proposed a time-frequency approach to evaluate GPR data for railway ballast assessment [9]. Their approach utilizes the short-time Fourier transform (STFT). Sinha *et al*. presented a new method for time-frequency map computation for non-stationary signals [15]. Their approach utilizes the continuous wavelet transform (CWT). Experiments on seismic data show that the CWT approach can be used to detect frequency shadows and subtle stratigraphic features. Fujimoto and Nonami suggested a mine detection algorithm based on statistical features, such as Student's *t*-distribution and chi-square distribution [16]. Their algorithm was shown to improve the probability of detection and decrease the probability of false alarm. Zoubir *et al*. compared a number of landmine detection techniques, such as Kalman filtering, background subtraction, matched filter de-convolution, wavelet packet decomposition and trimmed average power [14]. They evaluated the techniques using receiver operating characteristic curves and computation time. The Kalman filtering approach was found to outperform other methods on detection rate, but it has the highest computational cost. The aforementioned studies mainly focus on improving visualization and clarity of GPR signals, and human intervention is still required to interpret the processed signals, which may introduce subjectivity and user-dependency into data analysis.

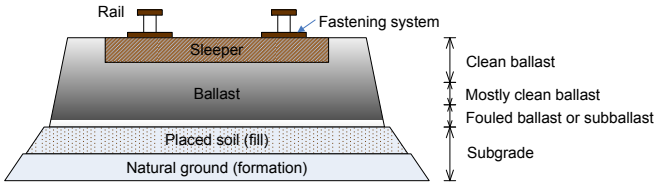

Fig. 1. Railway structure [9, 11].

In a GPR survey, because particular resonance frequencies arise in wave propagation, reflected waves from different buried objects or paths present different electromagnetic characteristics. Hence, it is possible to classify the buried objects or underground materials by analyzing the frequency spectra of the received GPR signals. Motivated by this observation, we propose a GPR signal classification system based on magnitude spectrum and support vector machines (SVMs) for ballast fouling assessment. The proposed system is designed so that no human intervention is required. It can automatically

extract and select features from GPR railway signals, and classify the GPR traces.

The remainder of the paper is organized as follows. In Section II, the proposed classification system is introduced. In Section III, the experimental methods and system implementation are explained. The experimental results are presented in Section IV, followed by some concluding remarks in Section V.

II. Proposed approach

In this section, we first give an overview of the GPR system, and then present the proposed approach for ballast fouling classification.

A. GPR system overview

Figure 2 illustrates the components of a typical GPR system. It consists of a signal generator (transmitter), transmitting and receiving antennas, and a recording device (receiver) [12, 17]. To detect objects, the transmitter generates a pulse and delivers it to the transmitting antenna T_x, which radiates an electromagnetic wave. Once the electromagnetic wave hits an object whose electrical properties are different from those of surrounding materials, part of the wave energy is reflected back towards the receiving antenna R_x. The detected energy is then sent to the receiver for storage and display.

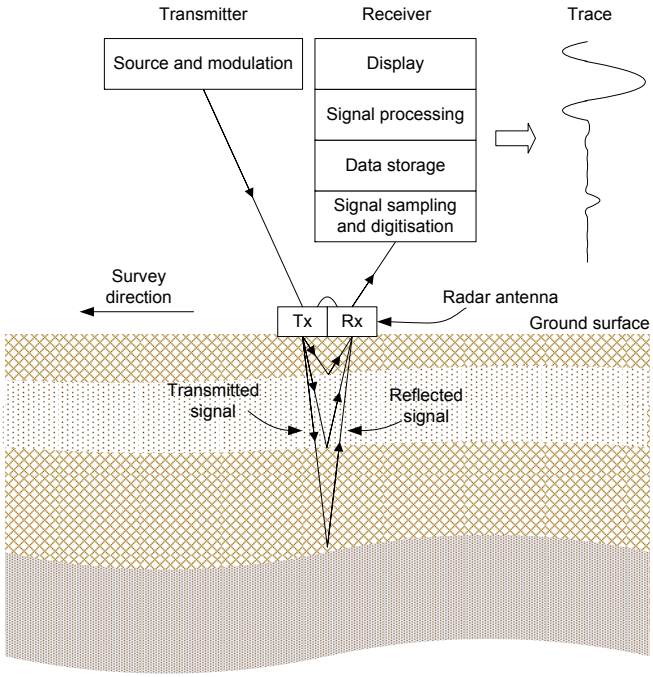

Fig. 2. GPR system components and GPR work process [12].

Since the GPR device can be mounted on a train, it is possible to conduct a continuous survey without interruption. With GPS devices and signal processing techniques, maintenance decisions can be made on site. A challenging task is how to interpret the GPR signals and assess the ballast condition automatically.

B. GPR trace classification system

Because the frequency spectrum of the GPR return reveals the characteristics of the materials on the electromagnetic wave path, we propose to use frequency features to automatically categorize ballast fouling conditions. Three traces from different fouling ballast are shown in Fig. 3, including their time-domain waveforms (Fig. 3a) and magnitude spectra (Fig. 3b). It is observed that the traces from ballast of different fouling conditions have different magnitude spectra. For example, the peak in the magnitude spectrum of the 50% clay is lower than the other two. In the frequency rage of 800 MHz to 1200 MHz, the magnitude spectrum of the 50% coal decays more rapidly than that of the clean ballast.

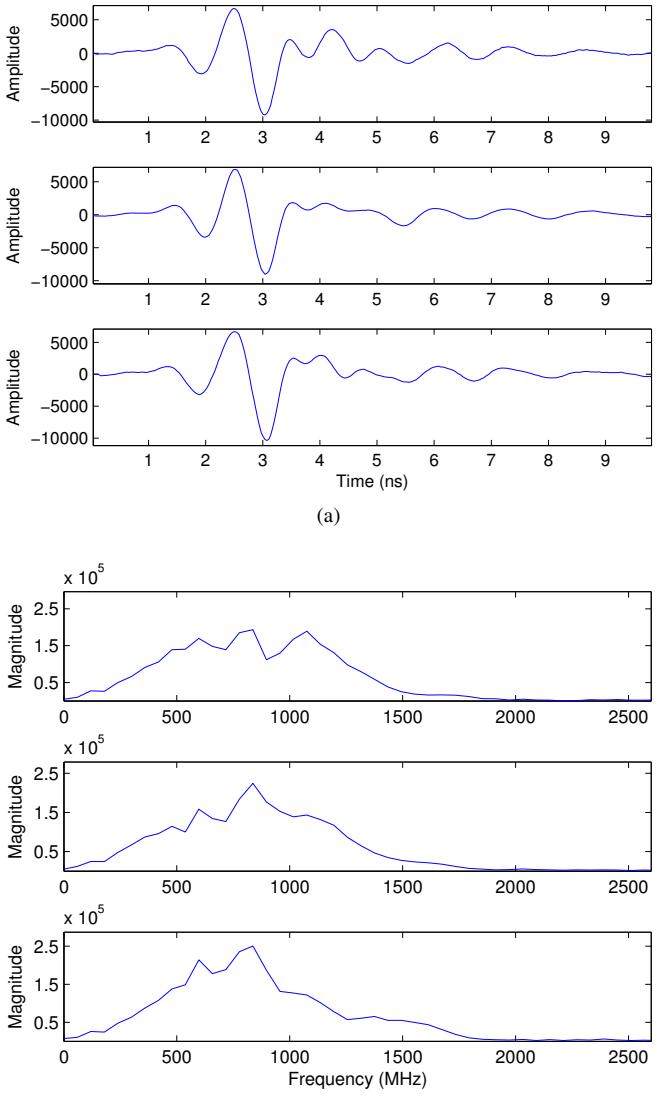

Fig. 3. Three traces from the railway data set. From top to bottom, they are from 50% clay ballast, clean ballast and 50% coal ballast, respectively. (a) Time-domain waveforms. (b) Frequency magnitude spectra.

The proposed automatic classification system includes three main stages: pre-processing, feature extraction, and classification. The system block diagram is shown in Fig. 4. When a GPR signal is received, salient features are extracted from

it automatically, and then sent to a pre-trained classifier for assessment of the railway ballast condition.

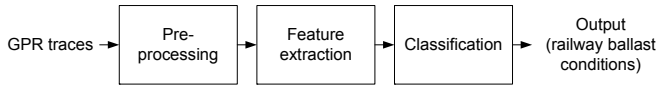

Fig. 4. Block diagram of the proposed automatic classification system.

C. Pre-processing and feature extraction

The pre-processing stage employs basic signal processing techniques, including DC component removal, re-sampling and time shifting, to reduce the intrinsic interferences introduced by the GPR and ensure the sampling rate consistency of the time-domain signals; depending on the system, samples located at the end of each trace may be discarded at this stage.

In the proposed system, feature extraction consists of three steps. First, the discrete Fourier transform is applied to GPR signals to obtain the magnitude spectra, which are normalized to ensure consistency in magnitude spectrum amplitudes. Second, salient frequencies are determined based on the training data and user-defined parameters. Third, feature vectors are formed by extracting magnitudes of local maxima and arranging them in ascending order of frequencies.

In the first step, the discrete Fourier transform (DFT) is applied to the time-domain trace. Let $s[n]$ be the discrete-time signal (real or complex) of length L obtained by sampling a continuous-time signal $s(t)$ with a uniform sampling rate f_s. The N-point DFT of $s[n]$ is defined as

$$S[k] = \sum_{n=0}^{N-1} s[n] e^{-j2\pi \frac{k}{N} n}, \quad k = 0, 1, 2, \cdots, N-1, \tag{1}$$

where $N \geq L$. Note that the analogue frequency corresponding to the k-th DFT index, $f(k)$, is given by

$$f(k) = \frac{k}{N} f_s, \quad k = 0, 1, 2, \cdots, N-1. \tag{2}$$

In the second step, the salient frequencies are determined. To reduce the dependency on the antenna gain, the magnitude spectrum is normalized as follows:

$$P_k = \frac{|S[k]|}{\sum_{k=0}^{N-1} |S[k]|/N}, \tag{3}$$

where $S[k]$ is the DFT coefficient computed in Eq. (1). Figure 5 shows the normalized magnitude spectra of traces obtained with an antenna frequency of 800 MHz. From this figure, it can be observed that the significant frequency components are below 2200 MHz, which is approximately three times the GPR antenna frequency. Similar observations can be made from the magnitude spectra of other GPR signals. The major frequency components of each trace reside mostly in the range $[0,\ 3f_a]$, where f_a is the antenna frequency. Therefore, the salient features of each trace can be extracted from this frequency range.

There are many frequencies that can be used in the range $[0,\ 3f_a]$. We choose the local maximum points within the specific frequency range as the salient frequencies. In our algorithm, the local maxima are located via the morphological operation *dilation*. Dilation is used because of its flexibility for local maxima search. Suppose that y is a 1-D discrete time signal and l is a flat structuring element, the dilation of y by l, denoted by $y \oplus l$, is defined as

$$[y \oplus l](x) = \max_{x' \in D_l} \{y(x - x')\}. \tag{4}$$

where D_l is the domain of l, and the structuring element is centered on x. Consequently, there are two adjustable parameters that determine the number of salient frequencies or the feature vector size: (i) the frequency distance between two adjacent local maxima, and (ii) the number of instances used to extract salient frequencies.

In the third step, the spectrum amplitudes at the selected frequencies are retrieved, and arranged in ascending order of frequencies to form a feature vector. In preliminary experiments, another frequency range $[0,\ 2f_a]$ was considered for feature extraction; however, using the same parameters, the classification rate was reduced for the frequency range $[0,\ 2f_a]$ compared to the frequency range $[0,\ 3f_a]$. Thus, $3f_a$ was chosen as the frequency boundary. On average, about half of the extracted features are found in the range $[2f_a,\ 3f_a]$.

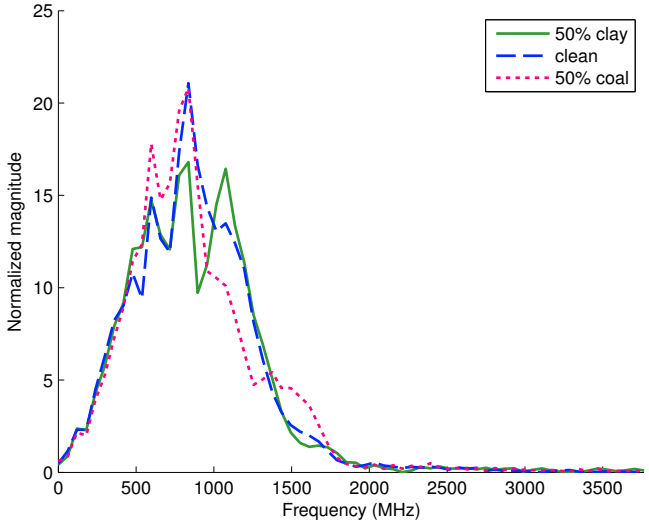

Fig. 5. Normalized magnitude spectra of three different traces obtained with 800 MHz antenna.

D. Classification using SVMs

There are many methods available for pattern classification, such as discriminant analysis [18], decision trees [19], k-nearest neighbors [18], Bayesian classifier [20], neural networks [21] and support vector machines [22]. Here, we choose support vector machines as the classification tool because they have been found to perform well in various practical applications [23, 24, 25]. Support vector machines are originally formulated for two-class classification problems. In SVMs, the decision boundary is obtained from the training data by finding a separating hyperplane that maximizes the margins between the two classes. This learning strategy is shown to increase the

generalization capability of the classifier. We can apply SVMs to complex non-linear problems by projecting the data onto a high-dimensional space using kernel methods.

Consider M training samples

$$\{(\mathbf{x}_1, y_1), (\mathbf{x}_2, y_2), \ldots, (\mathbf{x}_M, y_M)\},$$

where $\mathbf{x}_i \in R^n$ is a feature vector and $y_i \in \{1, -1\}$ is the class label. If the classes are linearly separable in the input space, the decision function can be written as

$$\begin{cases} \langle \mathbf{w}, \mathbf{x}_i \rangle + b \geq 1 & \text{for } y_i = 1, \\ \langle \mathbf{w}, \mathbf{x}_i \rangle + b \leq -1 & \text{for } y_i = -1, \end{cases} \tag{5}$$

or

$$y_i(\langle \mathbf{w}, \mathbf{x}_i \rangle + b) \geq 1, \tag{6}$$

where $\mathbf{w}$ is the vector normal to the hyperplane, b is a bias term, and $\langle \mathbf{w}, \mathbf{x} \rangle$ is the dot product of the vectors $\mathbf{w}$ and $\mathbf{x}$.

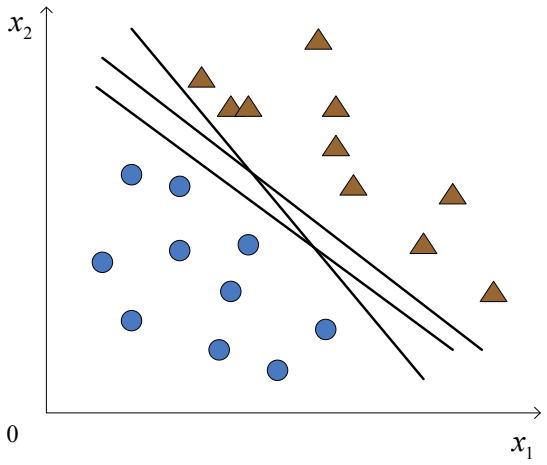

(a) Hyperplanes

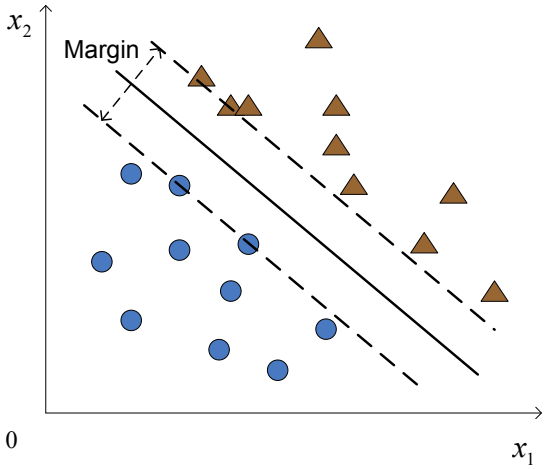

(b) Optimal hyperplane (solid line)

Fig. 6. SVM optimal hyperplane for a two-class problem. (a) The data can be separated by many hyperplanes. (b) Only one hyperplane achieves the maximum separation.

There are many hyperplanes that can separate the data (Fig. 6a). However, only one hyperplane, called *optimal separating hyperplane*, can achieve *maximum margin* (represented with the solid line in Fig. 6b). The margin perpendicular to the hyperplane can be expressed as $2/\|\mathbf{w}\|$. Consequently, the problem is to find $\mathbf{w}$ and b that maximize the margin. This is equivalent to minimizing

$$J(\mathbf{w}) = \frac{1}{2}\|\mathbf{w}\|^2, \tag{7}$$

subject to

$$y_i(\langle \mathbf{w}, \mathbf{x} \rangle + b) \geq 1 \text{ for } i = 1, \ldots, M. \tag{8}$$

If the classes are not separable, it is necessary to introduce non-negative slack variables ξ_i into constraint (8):

$$y_i(\langle \mathbf{w}, \mathbf{x} \rangle + b) \geq 1 - \xi_i. \tag{9}$$

A classifier that generalizes well can be found by minimizing

$$\tau(\mathbf{w}, \boldsymbol{\xi}) = \frac{1}{2}\|\mathbf{w}\|^2 + C\sum_{i=1}^{M} \xi_i, \tag{10}$$

subject to

$$y_i(\langle \mathbf{w}, \mathbf{x} \rangle + b) \geq 1 - \xi_i \text{ for } i = 1, \ldots, M, \tag{11}$$

where C is a constant representing the trade-off between margin maximization and training error minimization. This is a constrained optimization problem. By introducing non-negative Lagrange multipliers α_i and β_i, the problem can be expressed as

$$\min_{\mathbf{w},b} \max_{\boldsymbol{\alpha},\boldsymbol{\beta}} L(\mathbf{w}, b, \boldsymbol{\xi}, \boldsymbol{\alpha}, \boldsymbol{\beta}) = \frac{1}{2}\|\mathbf{w}\|^2 + C\sum_{i=1}^{M} \xi_i - \sum_{i=1}^{M} \alpha_i[y_i(\langle \mathbf{w}, \mathbf{x}_i \rangle + b) - 1 + \xi_i] - \sum_{i=1}^{M} \beta_i \xi_i. \tag{12}$$

The optimal solution should satisfy the following Karush-Kuhn-Tucker conditions [23, 26]

$$\frac{\partial}{\partial \mathbf{w}} L(\mathbf{w}, b, \boldsymbol{\xi}, \boldsymbol{\alpha}, \boldsymbol{\beta}) = 0, \tag{13}$$

$$\frac{\partial}{\partial b} L(\mathbf{w}, b, \boldsymbol{\xi}, \boldsymbol{\alpha}, \boldsymbol{\beta}) = 0, \tag{14}$$

$$\frac{\partial}{\partial \boldsymbol{\xi}} L(\mathbf{w}, b, \boldsymbol{\xi}, \boldsymbol{\alpha}, \boldsymbol{\beta}) = 0, \tag{15}$$

$$\alpha_i[y_i(\langle \mathbf{w} \cdot \mathbf{x}_i \rangle + b) - 1 + \xi_i] = 0 \text{ for } i = 1, \ldots, M, \tag{16}$$

$$\beta_i \xi_i = 0 \text{ for } i = 1, \ldots, M, \tag{17}$$

$$\alpha_i \geq 0,\ \beta_i \geq 0,\ \xi_i \geq 0 \text{ for } i = 1, \ldots, M. \tag{18}$$

Equations (13) to (18) lead to

$$\mathbf{w} = \sum_{i=1}^{M} \alpha_i y_i \mathbf{x}_i, \tag{19}$$

$$\sum_{i=1}^{M} \alpha_i y_i = 0, \tag{20}$$

and

$$\alpha_i + \beta_i = C. \tag{21}$$

Substituting Eqs. (19) to (21) into (12), the primal variables $\mathbf{w}$ and b can be eliminated and a dual optimization problem is obtained:

$$\text{maximizing } Q(\alpha) = \sum_{i=1}^{M} \alpha_i - \frac{1}{2} \sum_{i,j=1}^{M} \alpha_i \alpha_j y_i y_j \langle \mathbf{x}_i, \mathbf{x}_j \rangle , \tag{22}$$

subject to

$$0 \leq \alpha_i \leq C \text{ for } i = 1, \ldots, M, \tag{23}$$

and

$$\sum_{i=1}^{M} \alpha_i y_i = 0 \text{ for } i = 1, \ldots, M. \tag{24}$$

In real-world applications, classes are usually not linearly separable in the input space, and the classifiers obtained in the original input space may not have high generalization ability for unknown data. Therefore, the data samples from the input space are usually projected onto a higher-dimensional dot product space via a mapping function Φ. The linear decision boundary constructed in the projected space yields a non-linear decision boundary in the input space (see Fig. 7).

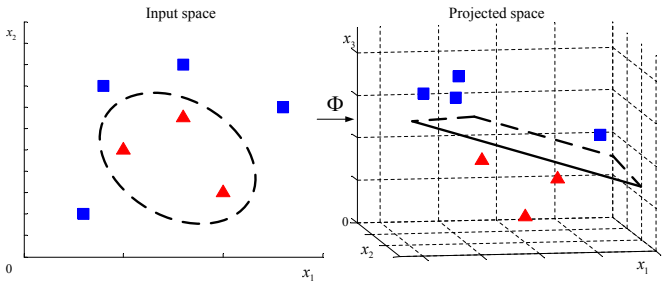

Fig. 7. By mapping data from the input space to a higher-dimensional space via Φ, it is possible to find a non-linear decision boundary in the original input space.

However, the projection is usually computation intensive. To simplify the projection, a positive semidefinite kernel H is employed:

$$H(\mathbf{x}, \mathbf{x}') = \langle \Phi(\mathbf{x}), \Phi(\mathbf{x}') \rangle. \tag{25}$$

Using the kernel, the dual problem in Eq. (22) is expressed as

$$\text{maximizing } Q(\alpha) = \sum_{i=1}^{M} \alpha_i - \frac{1}{2} \sum_{i,j=1}^{M} \alpha_i \alpha_j y_i y_j H(\mathbf{x}_i, \mathbf{x}_j), \tag{26}$$

subject to the constraints in (23) and (24).

Compared with several other kernels (linear and polynomial), the radial basis function (RBF) kernel has been chosen because it performs nonlinear mapping, and has less hyperparameters than the polynomial kernel; it is given by

$$H(\mathbf{x}, \mathbf{x}') = e^{-\gamma \left\| \mathbf{x} - \mathbf{x}' \right\|^2}, \tag{27}$$

where γ is a positive scalar. In this paper, we focus on support vector machines with RBF kernels.

III. Experimental Methods

The GPR operation along the railway can be affected by many factors, such as cross winds due to high speed rail, high electromagnetic interference and radio frequency interference from railway communications and automation, geomagnetic storms and thunderstorms [27]. To collect real-world data for system evaluation, we conducted GPR surveys along an existing railway track at Wollongong station in New South Wales, Australia. We have collected 25 920 GPR traces, of which 5 896 are with known ground truth. In this section, first we introduce the railway track and experimental set-up, then we explain the implementation of the proposed system.

A. Railway ballast data collection using GPR

Figure 8 shows the data collection equipment and the railway track where the experiments were conducted. This track is parallel to several tracks that are in service. Considering the time and cost, three sections with known ground truth of the railway track were chosen for the GPR data. Each section has a length of 2.0 m and a depth of 0.55 m; the width is equivalent to the existing ballast width. We excavated the long-standing ballast from these sections, then filled them with different types of ballast that were pre-mixed. Each section contained only one type of ballast. The sleepers were not reinstalled and the rails remained untouched.

The three ballast types are chosen based on the most common ballast fouling conditions: (i) 50% clay fouling, (ii) clean, and (iii) 50% coal fouling. Here, the percentage of fouling is a *relative ballast fouling ratio*; it represents the proportion of fouling particles to ballast particles [28]. Compared to the traditional *fouling index* and *percentage void contamination*, the relative ballast fouling ratio can reveal the effect introduced by specific gravity and gradation of fouling materials.

Before GPR surveys are conducted, a proper GPR system must be chosen based on the survey environment, budget and GPR system availability. To obtain quality GPR profiles, several factors were considered in choosing the appropriate antenna system, such as the depth to the bottom of ballast, resolution for ballast gravel grain size and fouling, operation environment, and the antenna height to avoid trash, sensors and switches [27]. Preliminary experiments were conducted to select the proper GPR antenna [29]. Different GPR systems from different companies were evaluated. Based on the results, the GPR system from MALÅ Geoscience was selected for data acquisition. The preliminary results also showed that the time-distance records from 800 MHz antenna were clearer than those from 1.2 GHz antenna. Therefore, our surveys mainly used the MALÅ 800 MHz antenna. The railway data collection system is illustrated in Fig. 8b, and the parameters of the ground penetrating radar used in the experiments are listed in Table I. Note that the bandwidth is approximately equal to the center frequency (antenna frequency).

The Wollongong railway data set consists of two parts: one collected under dry ground condition and the other gathered under wet condition.

(a)

(b)

Fig. 8. Experimental set-up: (a) an existing railway track used for GPR data collection; (b) the GPR data collection system.

TABLE I
RADAR PARAMETER CONFIGURATIONS FOR 800 MHZ ANTENNA USED IN THE SURVEYS.

Antenna height (mm)	Sampling frequency (MHz)
200	16477
	20401
	25201
	30601
300	16477
	20401
	25201
	30601
400	20401

- The dry ground data samples were acquired during sunny weather conditions; the materials filled in the three sections were also dry. Two antennas of center frequencies 800 MHz and 1.2 GHz from MALÅ Geoscience were deployed, each at two different heights: 200 mm and 300 mm. The antenna elevations can prevent collision of the ground penetrating radar with a variety of devices along the railway. Different GPR configuration parameters, including antenna height, time window and sampling frequency, were utilized. Twenty-four GPR profiles were collected with the antenna frequency of 800 MHz and 12 profiles with 1.2 GHz. Each profile contains the GPR signals for an entire section (50% clay, clean or 50% coal).
- The wet ground data set was obtained under cloudy weather conditions; heavy rains from the previous night saturated the materials. Only the antenna of center frequency 800 MHz was used. All radar profiles shared the same GPR configuration parameters. The antenna height was lifted to 400 mm to avoid obstacles along the railway track.

A summary of the Wollongong railway data set using 800 MHz antenna is presented in Table II. This data set, namely the combined 800 MHz data set, can be divided into three subsets based on the antenna heights:

1) 200 mm data subset,
2) 300 mm data subset, and
3) 400 mm data subset.

Each data subset consists of GPR traces from three different types of ballast. To reduce the border effects, the first and last 15% traces of each GPR profile were discarded.

TABLE II
NUMBERS OF AVAILABLE TRACES IN COMBINED 800 MHZ DATA SET.

Condition	**Dry**		**Wet**
Antenna height	200 mm	300 mm	400 mm
Section clay	469	470	745
Section clean	477	478	642
Section coal	436	438	705
Total	1382	1386	2092

B. System implementation

In the pre-processing phase, an automatic DC offset is applied to each trace to obtain a zero-mean signal. Next, every GPR trace is re-sampled to ensure data consistency. Then, each trace is shifted according to the position of the global maximum point. The shifting reduces the effects of antenna height variations; a few samples may be discarded from the end of each trace, based on the minimum trace length after re-sampling.

For feature extraction, the fast Fourier transform algorithm is applied to obtain the amplitude spectra. After normalization, several traces are selected to find the feature points, i.e. the salient frequencies in the range $[0,\ 3f_a]$. The magnitude spectrum features are extracted at these points to form the feature vector, which is fed to the classifier. Consider the three example traces in Fig. 5, representing three different ballast types. Each trace has a length of 308 in the discrete time domain. The magnitude spectra of the tree traces and the salient frequencies are shown in Fig. 9. In the figure, each vertical dotted line indicates a frequency where a magnitude feature is extracted. There are 17 feature points in this example, hence each trace is represented by a feature vector of size 17.

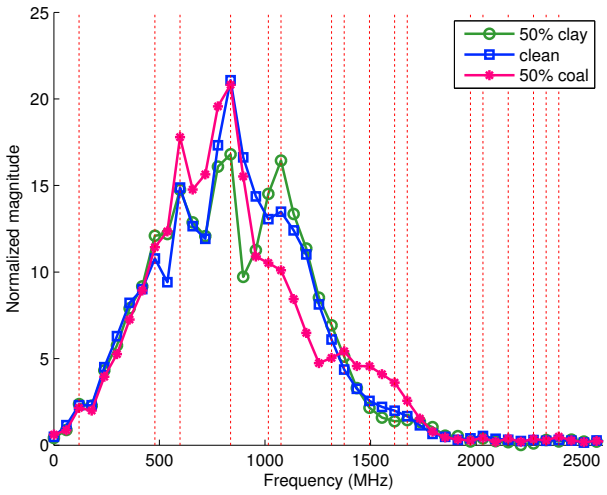

Fig. 9. Feature points of the three traces shown in Fig. 3a. Each vertical dotted line represents a feature point.

To train and test the SVM classifiers, the *LIBSVM* tool, developed by Chang *et al*. [30], was used. When building SVM classifiers, an exhaustive search for optimal SVM training parameters is computation-intensive. Thus, a hierarchical approach is applied in our system to reduce the computation cost. First, the parameter search is performed on a coarse grid. Once a possible region containing the optimal parameters is identified, a finer search is applied within the identified region. Compared to the exhaustive search, the two-level hierarchy reduces the training time by half. During training, the system sometimes finds more than one set of optimal parameters. To solve this, we simply construct a number of classifiers using the chosen parameters and form them as an SVMs pool [31]. Whenever a test sample is input into the system, it will be evaluated by every SVM classifier in the pool; a majority voting strategy is then applied to obtain the overall classification result.

SVMs utilize explicit decision functions and are formulated for two-class problems. It is necessary to extend the SVM formulation to handle multi-class problems. There are several ways to extend SVMs; one-versus-all and pair-wise are two common approaches. In this paper, we focus on the one-verus-all approach, and give results of the pair-wise SVM approach only for comparison purposes.

- In the one-versus-all approach, a k-class problem is decomposed into k two-class problems [23, 32]. Each SVM is trained with all the training samples. For the i-th SVM, where $i \leq k$, samples in the i-th class are labeled as positive, and samples in all other classes are labeled as negative. Note that the classifier parameters that yield high generalization are automatically selected using five-fold cross-validation on the training set.
- The pair-wise approach requires $k(k-1)/2$ two-class SVM classifiers to solve a k-class problem. Each SVM classifier is trained with samples from two classes. Let c_{ij} be the SVM classifier that is trained on data from the i-th and j-th classes. In the test phase, the SVM classifier c_{ij} $(i < j)$ divides all the data into class i and class j. The final classification results of pair-wise SVMs are obtained by combining all two-class classifiers with a majority voting scheme. For an input instance $\mathbf{x}$, if a pair-wise SVM classifier categorizes $\mathbf{x}$ in the k-th class, then the vote for class k is increased by one. Once all classifiers have voted, the pattern $\mathbf{x}$ is assigned to the class that has the highest voting score.

To evaluate the generalization ability of the classifiers, *cross-validation* is used. There are several methods of cross-validation; in the proposed system, we employ five-fold cross-validation. The entire data set is randomly divided into five partitions of approximately equal size. Four partitions are used to train, and the remaining partition is used to validate the classifier. The step is repeated five times until all partitions have been evaluated. Finally, the average classification rate across five folds is computed and used to measure the system performance.

IV. Results and Analysis

The proposed system is used to classify ballast fouling conditions. In Section IV-A, we present the experimental results using different numbers of salient frequencies with one-verus-all SVMs trained and tested on the the entire 800 MHz data set. In Section IV-B, we present the experimental results using the three data subsets. In Section IV-C we show the system performance on the 1.2 GHz data. In Section IV-E, we compare the one-versus-all SVMs with pair-wise SVMs, and discuss the advantages and disadvantages of these two multi-class SVM approaches. Then, the system is compared with the k-nearest neighbors algorithm and the Mahalanobis distance classifier using the proposed magnitude feature. A comparison is also made between the proposed feature extraction method and the STFT spectrogram.

A. Classification performance on the combined data set

In the first experiment, the proposed classification system is trained and tested on the combined data subsets collected with the 800 MHz antenna at different heights: 200 mm, 300 mm and 400 mm. The proposed feature extraction approach searches for local maximum points in the magnitude spectra; these points determine the corresponding salient frequencies. Our experiments show that it is not necessary to use all local maxima for classification. Thus, in the following, we analyze how the number of salient frequency points affects the system performance. Note that the number of frequency points is equivalent to the feature vector size.

There are two parameters that control the number of prominent frequencies: the distance between peaks and the number of traces used. In system evaluation, these two factors are both varied from 3 to 18. If there exist more than one pair of parameters that bear the same number of salient frequencies, the median classification rate is reported. The classification rate is the percentage of test samples that are correctly classified.

The classification performance on the combined 800 MHz data set using five-fold cross-validation is shown in Table III. The proposed system can achieve a classification rate of 99.5% with 7 salient frequencies, and 99.7% with 14 frequencies.

TABLE III
CLASSIFICATION RATES FOR DIFFERENT NUMBERS OF SALIENT FREQUENCIES ON THE COMBINED 800 MHZ DATA SET.

Number of salient frequencies	7	8	10	11	14	20	24
Overall classification rate (%)	99.5	99.6	99.6	99.8	99.7	100.0	100.0
Number of salient frequencies	29	30	31	32	33	34	-
Overall classification rate (%)	100.0	100.0	100.0	100.0	100.0	100.0	-

B. Classification performance versus antenna height

Further experiments have been conducted to explore the system performance on the three data subsets of different antenna heights. The three experiments using 800 MHz data set are:

1) training and testing on the 200 mm data subset,
2) training and testing on the 300 mm data subset, and
3) training and testing on the 400 mm data subset.

Since the salient frequency points are determined from the training data, the feature vectors are different for each experiment.

- The system classification performance on the 200 mm data subset as a function of the number of salient frequencies is given in Table IV. The system performance improves when more frequency points are used. When fewer than 5 frequency points are used, the classification rate is below 80.0%. When the number of frequency points reaches 5, the classification rate increases to 90.4%. Once the feature size reaches 14, the system performance remains stable with a classification rate above 99.0%. Perfect classification is achieved with 17 frequencies or higher.
- Table V shows the classification rates when the system is trained on the 300 mm data subset. The classification rate improves steadily with increasing number of salient frequencies. When the number of salient frequencies reaches 12, the system is able to classify the test set with a classification rate of 99.8%.
- For 400 mm antenna height data, the system achieves an overall classification rate of 99.7% with only 8 salient frequencies (see Table VI); the classification rate reaches 100.0% with 10 features.

The classification rates for the three data subsets are compared in Fig. 10. The experimental results show that the system performance varies with different numbers of salient frequencies; the classification rate tends to increase when more frequency points are used. When fewer salient frequency points are used, the system trained with 400 mm antenna height data performs better than the ones trained with 200 mm and 300 mm antenna height data. A possible explanation is that the 400 mm data were collected under a water saturated condition. The higher dielectric permittivity of the water results in a stronger reflection than the dry ballast. Although the distance between peaks and the number of traces are both varied from 3 to 18 for each experiment, the system is able to detect more points in the 400 mm data subset. For example, using the same range of parameters, more frequency points are extracted from the 400 mm data subset than from the other two subsets: 25 frequency points are extracted from the 200 mm data subset, 28 from the 300 mm subset, and 50 from the 400 mm subset. This can also be explained by the stronger reflection of the 400 mm data.

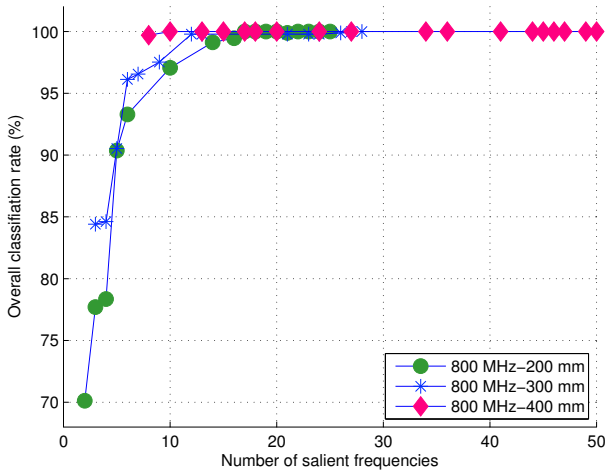

Fig. 10. Classification rates for different feature vector sizes and antenna heights.

We also analyzed the system performance when it was trained on data collected with one antenna height and tested on data collected with another antenna height. The results show that the classification rate decreases. However, the system performed well when it was trained and tested on mixed data of different antenna heights (see Table III). This shows that the proposed system can operate at different antenna heights, provided that the training data set is representative.

C. Analysis of operating antenna frequency

As mentioned in Section III-A, the MALÅ 1.2 GHz antenna was employed during the first survey. For comparison purposes, the classification performance for this antenna is shown in Table VII. When fewer than 16 frequency points are used, the classification rate is below 90.0%. When the feature vector size reaches 21, the classification rate reaches 95.7%. A classification rate of 99.0% requires a feature vector size of 30 or more. The results show that, when a small number of frequency points are used, the classification rate for the 1.2 GHz data is lower than the classification rate for the 800 MHz data. For example, the 1.2 GHz system requires 19 salient frequencies to achieve a classification rate of 93.0%, whereas the 800 MHz 200 mm system needs only 6 salient frequencies to obtain a similar classification rate (see Table IV). In GPR, low antenna frequencies penetrate deeper than high frequencies, while high frequencies provide finer resolution than the low frequencies [33]. The choice of antenna frequency is a trade-off between the required

TABLE IV
CLASSIFICATION RATES FOR DIFFERENT NUMBERS OF SALIENT FREQUENCIES. DATA SET: $f_a = 800$ MHz, $h = 200$ MM.

Number of salient frequencies	2	3	4	5	6	10	14	16
Overall classification rate (%)	70.1	77.7	78.4	90.4	93.3	97.1	99.1	99.5
Number of salient frequencies	17	18	19	20	22	23	24	25
Overall classification rate (%)	100.0	100.0	100.0	100.0	100.0	100.0	100.0	100.0

TABLE V
CLASSIFICATION RATES FOR DIFFERENT NUMBERS OF SALIENT FREQUENCIES. DATE SET: $f_a = 800$ MHz, $h = 300$ MM.

Number of salient frequencies	3	4	5	6	7	9	12
Overall classification rate (%)	84.4	84.6	90.5	96.1	96.6	97.5	99.8
Number of salient frequencies	13	21	23	24	26	27	28
Overall classification rate (%)	99.8	99.8	99.8	99.8	99.9	100.0	100.0

TABLE VI
CLASSIFICATION RATES FOR DIFFERENT NUMBERS OF SALIENT FREQUENCIES. DATE SET: $f_a = 800$ MHz, $h = 400$ MM.

Number of salient frequencies	8	10	13	15	17	18	20	24	27
Overall classification rate (%)	99.7	100.0	100.0	100.0	100.0	100.0	100.0	100.0	100.0
Number of salient frequencies	34	36	41	44	45	46	47	49	50
Overall classification rate (%)	100.0	100.0	100.0	100.0	100.0	100.0	100.0	100.0	100.0

TABLE VII
CLASSIFICATION RATES FOR DIFFERENT NUMBERS OF SALIENT FREQUENCIES. DATA SET: $f_a = 1.2$ GHz, $h = 200$ MM.

Number of salient frequencies	4	7	8	9	10	11	12	15	16	19	21
Overall classification rate (%)	48.3	77.5	77.2	75.9	83.2	86.2	84.8	88.1	88.1	93.0	95.7
Number of salient frequencies	24	25	26	27	28	29	30	31	32	34	-
Overall classification rate (%)	95.4	96.7	94.1	97.1	94.4	97.6	99.4	99.4	98.9	99.4	-

depth and resolution. In this case, the results indicate that the 1.2 GHz antenna is not as good as the 800 MHz antenna.

D. Analysis of SVM design

This section compares the performances of one-versus-all and pair-wise SVMs. With the one-versus-all SVM approach, if a sample is classified as positive by more than one classifier or negative by all classifiers, it will be labeled as unclassified. The unclassifiable regions of the one-versus-all approach are shown in Fig. 11. Pair-wise SVMs, on the other hand, have a smaller unclassifiable area compared to one-versus-all SVMs [23]. When a new ballast class is added to the system, the one-versus-all approach requires re-training all the classifiers, while the pair-wise approach involves training new classifiers between the added class and existing classes only.

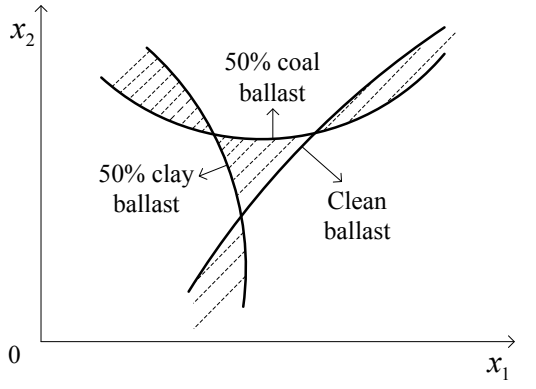

Fig. 11. An example of unclassifiable regions using one-versus-all SVMs. The solid lines are the class boundaries and the shaded regions represent the unclassifiable areas.

Consider samples that do not carry sufficient resonances. The one-versus-all system will not classify these samples into the predefined classes (50% clay, clean, and 50% coal). However, the pair-wise system will assign incorrect class labels to these samples. The overall classification rates of the two SVM systems on the combined 800 MHz data set are shown in Fig. 12. The performances of one-versus-all and pair-wise SVMs are nearly the same.

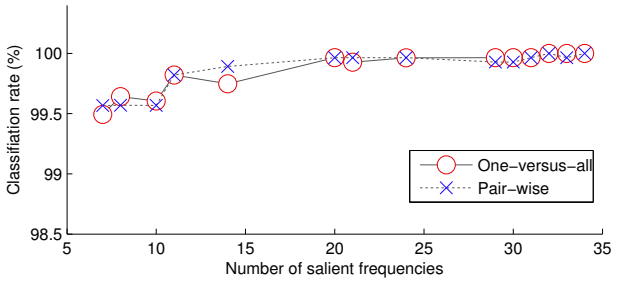

Fig. 12. Comparison of classification rates between one-versus-all SVMs and pair-wise SVMs.

E. Comparison with other approaches

In this section, we compare the performance of the proposed classification system with those of the k-nearest neighbors (k-NN) and the Mahalanobis classifiers, using the same data set. We also compare the proposed magnitude spectrum features with features extracted from the STFT spectrogram.

1) Comparison with k-NN and Mahalanobis distance classifier:

The k-nearest neighbor classifier is a supervised learning

algorithm based on sample distances [18]. It classifies a new sample by searching for the closest training samples. The label of the new sample is decided via a majority voting scheme based on the labels of the k nearest neighbors. In our implementation, k was varied from 1 to 17 in steps of 2.

The Mahalanobis distance is a statistical distance measure that takes into account correlation between variables. First, the mean $\mathbf{m}_i$ and the covariance matrix $\mathbf{C}_i$ of each class are computed from the training population. For an observation $\mathbf{x}$ to be classified, the Mahalanobis distance between $\mathbf{x}$ and each class is computed as follows:

$$D_i(\mathbf{x}, \mathbf{m}_i) = \sqrt{(\mathbf{x} - \mathbf{m}_i)\mathbf{C}_i^{-1}(\mathbf{x} - \mathbf{m}_i)^T}. \quad (28)$$

where i denotes the class index. The sample $\mathbf{x}$ is assigned to the class with the smallest Mahalanobis distance; that is, the index of the winning class i^* is given by

$$i^* = \arg\min_i (D_i). \quad (29)$$

For comparison, five-fold cross-validation was applied. The number of frequencies for the three 800 MHz data subsets were 10, 9, and 8, respectively. Parameter k for the k-NN classifier was chosen based on the training data set.

The results are shown in Fig. 13. For the 200 mm and 400 mm antenna heights, the overall classification rates of the k-NN classifier are superior to those of the Mahalanobis distance classifier. With the 300 mm antenna height data, the k-NN classifier and the Mahalanobis distance classifier have close performance. For all the data subsets, the one-versus-all SVMs outperform both the k-NN and the Mahalanobis distance classifier in terms of overall classification rate. For example, on the 300 mm data subset, the SVM classifier achieves a classification rate of 97.5%, while the k-NN and the Mahalanobis distance classifiers reach 95.1% and 94.9%, respectively.

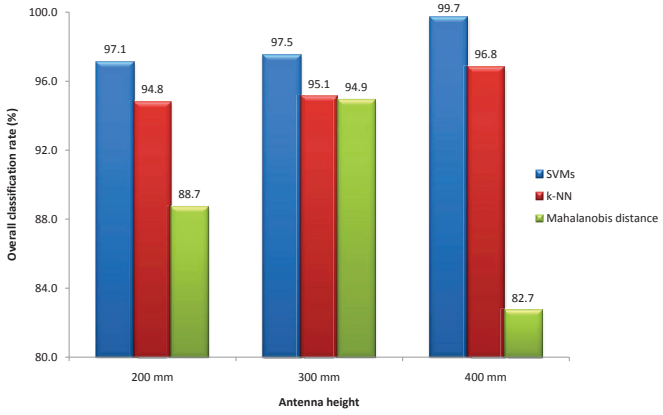

Fig. 13. Comparison of SVM, k-NN ($k = 15$) and Mahalanobis distance classifiers. Data set: $f = 800$ MHz.

2) Comparison with STFT spectrogram:

In [9], Al-Qadi *et al.* proposed a time-frequency approach using short-time Fourier transform. The energy attenuation of STFT spectrogram is utilized to assess ballast conditions. However, their approach requires visual inspection. Here, we are interested in the classification performance of the STFT spectrogram features when used in the proposed system.

Our STFT spectrogram implementation is shown in Fig. 14. The GPR traces are pre-processed, and the discrete-time STFT is then applied to obtain the spectrogram. The discrete-time STFT is defined as

$$X(m, \omega) = \sum_{n=-\infty}^{\infty} x[n]w[n-m]e^{-j\omega n}, \quad (30)$$

where $X(m, \omega)$ is the STFT of windowed data, $x[n]$ is a GPR trace, and $w[n]$ is a window function. The spectrogram is represented by a 2-D matrix whereas the SVMs accept a 1-D feature vector only. Therefore, the spectrogram is converted into a row vector. Furthermore, considering the computational complexity, we downsample the row vector to a feature vector of 16, 32, 64, 128 or 256 elements. Next, the extracted feature vectors are used as inputs to one-versus-all SVMs.

The results on the combined 800 MHz data set are shown in Table VIII. The STFT spectrogram requires 128 frequency points to achieve an overall classification rate of 92.9%; while the proposed magnitude spectra yield a classification rate of 99.5% using only 7 frequency points.

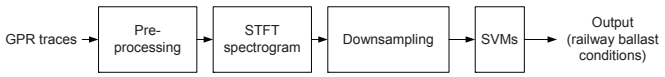

Fig. 14. Block diagram of the STFT spectrogram implementation.

TABLE VIII
CLASSIFICATION RATES FOR STFT SPECTROGRAM FEATURE. DATA SET: COMBINED 800 MHZ DATA SET.

Feature vector size	16	32	64	128	256
Overall classification rate (%)	68.3	70.8	76.0	92.9	88.1

V. CONCLUSION

Compared with the traditional approach, GPR provides a non-destructive and mobile means for fouling assessment of railway ballast. In this paper, we have presented an automatic classification system for GPR traces. The proposed system is based on magnitude spectrum analysis and support vector machines; it automates the entire GPR signal processing and interpretation. Real-world railway data of three common ballast fouling conditions (clean ballast, 50% clay ballast and 50% coal ballast) were collected to evaluate the proposed system. We have made the comparison between the proposed salient magnitude spectra and the STFT spectrogram, and between SVMs and other two common classifiers. The experimental results indicate that (i) the proposed salient spectrum amplitudes are an efficient representation of ground penetrating radar signals; (ii) the system performs well in ballast fouling classification, for example, on the combined 800 MHz data set, the system can achieve a classification rate of 99.5% using 7 salient frequencies; and (iii) the system can operate with different antenna heights, such as 200 mm, 300 mm and 400 mm, provided that the training data set is representative of antenna height variations.

ACKNOWLEDGMENTS

This work is supported in part by a grant from the *Australian Research Council*. The railway GPR data were collected as part of the Rail CRC-AT5 project, sponsored by *CRC Rail for Innovation*.

REFERENCES

[1] A. P. Annan, "GPR - history, trends, and future developments," *Subsurface Sensing Technologies and Applications*, vol. 3, no. 4, pp. 253–270, 2002.

[2] D. J. Daniels, Ed., *Ground Penetrating Radar*, 2nd ed. London: The Institution of Electrical Engineers, 2004.

[3] D. J. Daniels, D. J. Gunton, and H. F. Scott, "Introduction to subsurface radar," *IEE Proceedings F, Radar and Signal Processing*, vol. 135, no. 4, pp. 278–320, 1988.

[4] A. Neal, "Ground-penetrating radar and its use in sedimentology: principles, problems and progress," *Earth-Science Reviews*, vol. 66, no. 3-4, pp. 261–330, 2004.

[5] M. Skolnik, Ed., *Radar Handbook*, 3rd ed. New York: McGraw-Hill, 2008.

[6] A. Denis, F. Huneau, S. Hoerl, and A. Salomon, "GPR data processing for fractures and flakes detection in sandstone," *Journal of Applied Geophysics*, vol. 68, no. 2, pp. 282–288, 2009.

[7] J. J. Degenhardt Jr, "Development of tongue-shaped and multilobate rock glaciers in alpine environments - interpretations from ground penetrating radar surveys," *Geomorphology*, vol. 109, no. 3-4, pp. 94–107, 2009.

[8] J. Francke, "Applications of GPR in mineral resource evaluations," in *13th International Conference on Ground Penetrating Radar (GPR)*, 2010, pp. 1–5.

[9] I. L. Al-Qadi, W. Xie, and R. Roberts, "Time-frequency approach for ground penetrating radar data analysis to assess railroad ballast condition," *Research in Nondestructive Evaluation*, vol. 19, no. 4, pp. 219 – 237, 2008.

[10] J. P. Hyslip, S. S. Smith, G. R. Olhoeft, and E. T. Selig, "Assessment of railway track substructure condition using ground penetrating radar," in *2003 Annual Conference of AREMA*, Chicago, 2003.

[11] A. Loizos and C. Plati, "Ground penetrating radar: A smart sensor for the evaluation of the railway trackbed," in *IEEE Instrumentation and Measurement Technology Conference Proceedings*, 2007, pp. 1–6.

[12] J. M. Reynolds, *An Introduction to Applied and Environmental Geophysics*. New York: John Wiley, 1996.

[13] H. M. Jol, Ed., *Ground Penetrating Radar Theory and Applications*, 1st ed. Amsterdam: Elsevier Science, 2009.

[14] A. M. Zoubir, I. J. Chant, C. L. Brown, B. Barkat, and C. Abeynayake, "Signal processing techniques for landmine detection using impulse ground penetrating radar," *IEEE Sensors Journal*, vol. 2, no. 1, pp. 41–51, 2002.

[15] S. Sinha, P. S. Routh, P. D. Anno, and J. P. Castagna, "Spectral decomposition of seismic data with continuous-wavelet transform," *Geophysics*, vol. 70, no. 6, pp. 19–25, 2005.

[16] M. Fujimoto, K. Nonami, A. Tatsuo, Y. Shigeru, and M. Kazuhisa, "Mine detection algorithm using pattern classification method by sensor fusion–experimental results by means of GPR," in *Systems and Human Science*. Amsterdam: Elsevier Science, 2005, pp. 259–274.

[17] B. J. Allred, J. J. Daniels, and M. R. Ehsani, Eds., *Handbook of Agricultural Geophysics*. Hoboken: CRC Press, 2008.

[18] C. M. Bishop, *Pattern Recognition and Machine Learning*. New York: Springer, 2006.

[19] R. O. Duda, P. E. Hart, and D. G. Stork, *Pattern Classification*, 2nd ed. New York: Wiley, 2001.

[20] S. L. Phung, A. Bouzerdoum, and D. Chai, "Skin segmentation using color pixel classification: analysis and comparison," *IEEE Transactions on Pattern Analysis and Machine Intelligence*, vol. 27, no. 1, pp. 148–154, 2005.

[21] S. L. Phung and A. Bouzerdoum, "A new image feature for fast detection of people in image," *International Journal of Information and Systems Sciences*, vol. 3, no. 3, pp. 383–391, 2007.

[22] W. Shao, G. Naghdy, and S. L. Phung, "Automatic image annotation for semantic image retrieval," in *Lecture Notes in Computer Science: VISUAL2007*, G. Qiu, Ed. Berlin Heidelberg: Springer-Verlag, 2007, vol. 4781, pp. 372–381.

[23] S. Abe, *Support Vector Machines for Pattern Classification*. New York: Springer, 2005.

[24] N. Cristianini and J. Shawe-Taylor, *An Introduction to Support Vector Machines and Other Kernel-based Learning Methods*. Cambridge: Cambridge University Press, 2001.

[25] M. A. Hearst, S. T. Dumais, E. Osman, J. Platt, and B. Scholkopf, "Support vector machines," *IEEE Intelligent Systems and Their Applications*, vol. 13, no. 4, pp. 18–28, 1998.

[26] B. Schlkopf and A. J. Smola, *Learning with Kernels: Support Vector Machines, Regularization, Optimization, and Beyond*, 1st ed. Cambridge, MA: The MIT Press, 2001.

[27] G. R. Olhoeft, "Working in a difficult environment: GPR sensing on the railroads," in *2005 IEEE Antennas and Propagation Society International Symposium*, vol. 3B, 2005, pp. 108–111.

[28] B. Indraratna, L. Su, and C. Rujikiatkamjorn, "A new parameter for classification and evaluation of railway ballast fouling," *Canadian Geotechnical Journal*, 2011, in press.

[29] W. Shao, A. Bouzerdoum, S. L. Phung, L. Su, B. Indraratna, and C. Rujikiatkamjorn, "Automatic classification of GPR signals," in *XIII International Conference on Ground Penetrating Radar*, Lecce, Italy, 2010.

[30] C.-C. Chang and C.-J. Lin, *LIBSVM: a library for support vector machines*, 2007. [Online]. Available: http://www.csie.ntu.edu.tw/~cjlin/libsvm/

[31] W. Shao, "Automatic annotation of digital photos," Master's thesis, University of Wollongong, 2007.

[32] V. N. Vapnik, *The Nature of Statistical Learning Theory*, 2nd ed. New York: Springer, 2000.

[33] C. Hauck and C. Kneisel, Eds., *Applied Geophysics in Periglacial Environments*. Leiden: Cambridge University Press, 2008.

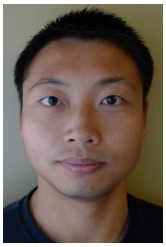

Wenbin Shao received the B.Eng degree (Communication Engineering) in 2003 from Northwestern Polytechnical University, Xi'an, China, and the M.Eng in 2007 from University of Wollongong, Wollongong, Australia. Currently he is a PhD student in the University of Wollongong.

Abdesselam Bouzerdoum is Professor of Computer Engineering and Associate Dean (Research), Faculty of Informatics, University of Wollongong, Australia. He received the M.Sc. and Ph.D. degrees, both in electrical engineering, from the University of Washington, Seattle, USA. He joined Adelaide University in July 1991, and he was promoted to Senior Lecturer (Senior Assistant Professor) in January 1995. In 1998, he was appointed Associate Professor at Edith Cowan University, Perth, Western Australia. In 2004, he moved to the University of Wollongong to take up the position of Professor of Computer Engineering and Head of School of Electrical, Computer and Telecommunications Engineering. In 2007, he was appointed Associate Dean (Research) in the Faculty of Informatics. Since 2009 he has been serving as a member of the Australian Research Council College of Experts, and Deputy Chair of the Engineering, Mathematics and Informatics Discipline since 2010.

Dr. Bouzerdoum received numerous awards and distinctions as acknowledgment of his research contributions. Most notable are a Distinguished Researcher (Chercheur de Haut Niveau) Fellowship from the French Ministry of Scientific Research in 2001 to conduct research at the LAAS/CNRS in Toulouse, two Vice Chancellor's Distinguished Researcher Awards, two awards for Excellence in Research Leadership, three awards for Excellence in Research Supervision, and the 2004 Chester Sall Award for best paper in IEEE Trans. on Consumer Electronics (3rd prize). He held several appointments as Visiting Professor at Institut Galilée, University of Paris-13 (2004, 2005, 2007, 2008 and 2010), Hong Kong University of Science and Technology (2007), and Villanova University (2010). He has published over 260 technical articles and graduated sixteen Ph.D. and seven Research Masters students. He served as Chair of the IEEE WA Section Signal Processing Chapter in 2004, and was Chair of the IEEE SA Section NN RIG from 1995 to 1997. From 1999 to 2006, he served as Associate Editor of IEEE Transactions on Systems, Man and Cybernetics. Currently, he is an Associate Editor of three international journals and a member of the governing board of the Asia Pacific Neural Network Assembly. Dr. Bouzerdoum is a senior member of IEEE, and a member of the Optical Society of America and INNS.

Son Lam Phung received the B.Eng degree with first-class honors in 1999, and the Ph.D. degree in 2003, all in computer engineering, from Edith Cowan University, Perth, Australia. He received the University and Faculty Medals in 2000. Dr. Phung joined the University of Wollongong as Research Fellow in 2005, and is currently a Senior Lecturer in the School of Electrical, Computer and Telecommunications Engineering. His general research interests are in the areas of image and video processing, neural networks, pattern recognition and machine learning.

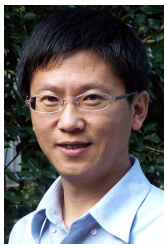

Lijun Su is a Research Fellow in the department of Civil, Mining & Environmental Engineering at University of Wollongong. He graduated from Xi'an Jiaotong University in China (BEng) in 2000 and obtained Masters degree (Meng) from the same university in 2002. He obtained his PhD in Geotechnical Engineering from the Hong Kong Polytechnic University in 2006. His areas of expertise include constitutive modelling of geotechnical materials and non-destructive inspection of underground conditions. He has published over 30 articles in international journals and conferences.

Buddhima Indraratna (FIEAust, FASCE, FGS, CEng, CPEng) is an internationally acclaimed geotechnical researcher and consultant. After graduating in Civil Engineering from Imperial College, University of London he obtained a Masters in Soil Mechanics also from Imperial College, and subsequently earned a PhD in geotechnical engineering from University of Alberta, Canada. He is currently Professor and Head, School of Civil, Mining & Environmental Engineering, University of Wollongong, Australia. His outstanding professional contributions encompass innovations in railway geotechnology, soft clay engineering, ground improvement, environmental geotechnology and geohydraulics, with applications to transport infrastructure and dam engineering. Under his leadership, Centre for Geomechanics & Railway Engineering at University of Wollongong has evolved to be a world class institution in ground improvement and transport geomechanics, undertaking national and international research and consulting jobs.

Recognition of his efforts is reflected by numerous prestigious Awards, such as: 2009 EH Davis Memorial Lecture by the Australian Geomechanics Society for outstanding contributions to the theory and practice of geomechanics and Australian Commonwealth government hosted 2009 Business-Higher Education Round Table award for Rail Track Innovations among others. He is the author of 4 other books and over 350 publications in international journals and conferences, including more than 30 invited keynote lectures worldwide. In the past, several of his publications have received outstanding contribution awards from International Association for Computer Methods and Advances in Geomechanics (IACMAG), Canadian Geotechnical Society and Swedish Geotechnical Society.

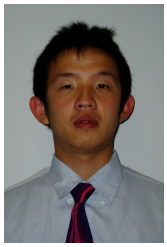

Cholachat Rujikiatkamjorn is a Senior Lecturer in Civil Engineering at University of Wollongong. He is a Civil Engineering graduate from Khonkaen University, Thailand (BEng) with a Masters (Meng) from the Asian Institute of Technology, Thailand. He obtained his PhD in Geotechnical Engineering from the University of Wollongong. His key areas of expertise include ground improvement for transport infrastructure and soft soil engineering. In 2009, he received an award from the International Association for Computer Methods and Advances in Geomechanics (IACMAG) for an outstanding paper by an early career researcher, and the 2006 Wollongong Trailblazer Award for innovations in soft soil stabilisation for transport infrastructure. He has published over 50 articles in international journals and conferences.